

RESEARCH ARTICLE

Cadmium Sulphide-Reduced Graphene Oxide-Modified Photoelectrode-Based Photoelectrochemical Sensing Platform for Copper(II) Ions

Ibrahim¹, H. N Lim^{1,2*}, N. M Huang³, A Pandikumar³

1 Department of Chemistry, Faculty of Science, Universiti Putra Malaysia, 43400 UPM, Serdang, Selangor, Malaysia, **2** Functional Device Laboratory, Institute of Advanced Technology, Universiti Putra Malaysia, 43400 UPM, Serdang, Selangor, Malaysia, **3** Low Dimensional Materials Research Centre, Department of Physics, Faculty of Science, University of Malaya, Kuala Lumpur, 50603, Malaysia

* hongnggee@upm.edu.my



OPEN ACCESS

Citation: Ibrahim I, Lim HN, Huang NM, Pandikumar A (2016) Cadmium Sulphide-Reduced Graphene Oxide-Modified Photoelectrode-Based Photoelectrochemical Sensing Platform for Copper(II) Ions. PLoS ONE 11(5): e0154557. doi:10.1371/journal.pone.0154557

Editor: Yogendra Kumar Mishra, Institute for Materials Science, GERMANY

Received: January 17, 2016

Accepted: April 17, 2016

Published: May 13, 2016

Copyright: © 2016 Ibrahim et al. This is an open access article distributed under the terms of the [Creative Commons Attribution License](https://creativecommons.org/licenses/by/4.0/), which permits unrestricted use, distribution, and reproduction in any medium, provided the original author and source are credited.

Data Availability Statement: All relevant data are within the paper and its Supporting Information files.

Funding: This research work was supported by a Wighton Titular Fellowship in Engineering (6385600-10501), HN Lim, and High Impact Research Grants (UM.C/625/1/HIR/MOHE/SC/21) from the Ministry of Higher Education, NM Huang. The funders had no role in study design, data collection and analysis, decision to publish, or preparation of the manuscript.

Competing Interests: The authors have declared that no competing interests exist.

Abstract

A photoelectrochemical (PEC) sensor with excellent sensitivity and detection toward copper (II) ions (Cu^{2+}) was developed using a cadmium sulphide-reduced graphene oxide (CdS-rGO) nanocomposite on an indium tin oxide (ITO) surface, with triethanolamine (TEA) used as the sacrificial electron donor. The CdS nanoparticles were initially synthesized *via* the aerosol-assisted chemical vapor deposition (AACVD) method using cadmium acetate and thiourea as the precursors to Cd^{2+} and S^{2-} , respectively. Graphene oxide (GO) was then dip-coated onto the CdS electrode and sintered under an argon gas flow (50 mL/min) for the reduction process. The nanostructured CdS was adhered securely to the ITO by a continuous network of rGO that also acted as an avenue to intensify the transfer of electrons from the conduction band of CdS. The photoelectrochemical results indicated that the ITO/CdS-rGO photoelectrode could facilitate broad UV-visible light absorption, which would lead to a higher and steady-state photocurrent response in the presence of TEA in 0.1 M KCl. The photocurrent decreased with an increase in the concentration of Cu^{2+} ions. The photoelectrode response for Cu^{2+} ion detection had a linear range of 0.5–120 μM , with a limit of detection (LoD) of 16 nM. The proposed PEC sensor displayed ultra-sensitivity and good selectivity toward Cu^{2+} ion detection.

1. Introduction

Copper (II) ions (Cu^{2+}) are the third most abundant transition metal ion and an essential trace element in the human body. Although Cu^{2+} ions are physiologically essential for various reasons, they are also an important environmental pollutant. The recommended allowance of copper is 0.8–0.9 mg/day for normal adults [1]. The drinking water quality guidelines by the World Health Organization (WHO) suggests that the amount of copper in drinking water should be

limited to 1.3 mg/L ($\sim 20 \mu\text{M}$) [2, 3]. Aberrant levels of copper exhibit significant deleterious effects on living organisms, such as Wilson's disease, pre-menstrual syndrome, adult polycystic kidney disease, fibroids, and infertility [3, 4]. As a result, there has been ongoing interest in developing better sensors for Cu²⁺ ion detection, because of their significance in the environment and biological systems. Although conventional methods such as chromatography-mass spectrometry, inductively coupled plasma mass spectrometry, and atomic absorption spectrometry are common detection tools, expensive instrumentation, extremely time-consuming processes, and the necessity of sophisticated operation have retarded their progress. Hence, the discoveries of sustainable techniques are needed to overcome the limitations. Recently, photoelectrochemical (PEC) has attracted much attention among researchers as a sensing platform for Cu²⁺ ion detection because it offers sensitive, fast, reproducible, simple, low-cost, and accurate potential alternatives to the above conventional methods.

PEC sensing is an approach that relies on photo-illumination to transfer electrons between an analyte, a semiconductor, and an electrode [5, 6]. A PEC sensor harnesses light to stimulate the photoactive species on the electrode, and utilizes a photocurrent as a means to quantify the changes. Furthermore, it has numerous inherent benefits such as a simple electronic circuit and easy fabrication, and it can use a low-power light source, which results in a very low instrumentation cost [7]. In order to further enhance the performance of PEC sensors, triethanolamine, ascorbic acid, and sodium sulphide are often added to the PEC detection cell as electron donors [8]. Semiconductors such as TiO₂ [9], ZnO [10] and CdS [11] can be used as the photoactive materials in the PEC sensor.

The photoactive material plays a major role in the PEC sensing performances for heavy metal ions. A PEC sensing system with high sensitivity can be achieved by amplifying the photocurrent intensity and minimizing the electron-hole recombination. Cadmium sulfide (CdS) semiconductor nanoparticles are the best candidate to achieve this target because of their application potential, based on size-tunable optical properties and high mobility [12]. CdS possesses a band gap of $\sim 2.4 \text{ eV}$, and has been considerably investigated for PEC sensing, as well as for the other visible-light-driven PEC applications [13]. In order to heighten the photocurrent generated by the CdS nanoparticles, it is essential to hold back the rapid recombination of the photogenerated electron-holes using CdS on support materials with large surface areas or by hybridizing CdS with conductive matrices such as carbon materials [14, 15].

As a flexible atom-thin 2D carbon material, graphene has emerged as a rising star because of its outstanding properties and excellent performance, including its very large surface area (theoretically, $2630 \text{ m}^2 \text{ g}^{-1}$ for a single-layer of graphene) [16], extraordinary electrical and thermal conductivities [17, 18], excellent mechanical strength [19] and good biocompatibility [20]. Considering its remarkable physical, chemical, and structural properties, materials based on graphene and its derivatives have sprung up quickly and been given tremendous attention across many disciplines, including novel nanoelectronics, high-frequency electronics, energy conversion and storage, biomedical devices, and sensors. Graphene-based electrochemical studies have received much interest because of its important role in accelerating electron transfer, with the merits of a high carrier mobility and exceptional electrical conductivity [21], which subsequently provide new opportunities to develop high-performance electrochemical sensors. To date, most graphene-based electrochemical sensors have used reduced graphene oxide (rGO) instead of graphene oxide (GO) because (i) it is rich in structural defects and its chemical groups facilitate the charge transfer process and thus enhance its electrochemical activity; (ii) the abundant chemical moieties on the rGO surface create availability and flexibility for various surface functionalizations, which boost the sensing performance; (iii) excellent tunable chemical and electrical properties; and (iv) efficient charge transport compared to non-conductive GO. The aforementioned benefits of rGO in electrochemical sensing can be

enhanced by assembling CdS nanoparticles on its surface to intensify the photocurrent performance through the synergic effects between CdS and rGO [21] in addition to addressing the photocorrosion problems of CdS nanoparticles, making this nanocomposite suitable for photoelectrochemical sensing. The present research focused on the development of an easy-to-use, economical, mobile, selective, and sensitive analytical approach for the detection of Cu²⁺ ions based on a photoelectrochemical technique. CdS semiconductor nanoparticles were synthesized on an indium tin oxide (ITO) electrode with an aerosol-assisted chemical vapor deposition (AACVD) procedure using Cd(CH₃COO)₂·2H₂O and CH₄N₂S as the precursors to Cd²⁺ and S²⁻, respectively. The rGO was then assembled on the CdS nanoparticles using a dip-coating method. The as-prepared ITO/CdS-rGO electrode was used for the detection of Cu²⁺ ions in an aqueous solution, in the presence of an electron donor, triethanolamine (TEA). It was found that the nanocomposites enhanced the photocurrent response up to 63 μA as a result of the rapid interfacial electron-transfer process. The results of this study demonstrated that the ITO/CdS-rGO photoelectrode has the potential to exhibit an excellent photocurrent response in 0.1 M of KCl under light illumination, which could provide a remarkable response upon the addition of Cu²⁺ ions. Based on the significant quenching in the photocurrent signal, an unconventional strategy was developed for the PEC detection of Cu²⁺ ions, with a linear concentration range of 0.5–120 μM, which gives a LoD of 16 nM.

2. Experimental Methods

2.1. Materials

Graphite flakes were purchased from Asbury Graphite Mills Inc., USA. Cadmium acetate dihydrate (Cd(CH₃COO)₂·2H₂O) and copper(II) sulfate pentahydrate (CuSO₄·5H₂O) were purchased from Hamburg Chemical. Thiourea (CH₄N₂S) was purchased from Fisher scientific. Methanol (CH₃OH, 99.9%) and acetone ((CH₃)₂CO, 99.5%) were purchased from Friendemann Schmidt. Ethanol (CH₃CH₂OH, 95%) was purchased from Systerm. Potassium chloride (KCl) was purchased from Merck. Triethanolamine (TEA, 99%) was received from R & M Chemicals. Indium tin oxide (ITO) conducting glass slides (7 Ωsq⁻¹) were commercially supplied by Xin Yan Technology Limited, China. Stock solutions of Cu²⁺, Ni²⁺, Co²⁺, Fe³⁺, Mn²⁺, Na⁺, K⁺, Ba²⁺, Zn²⁺, Mg²⁺, and Al³⁺ were prepared by dissolving suitable amounts of the CuSO₄, NiSO₄, CoSO₄, Fe(NO₃)₃, MnCl₂, NaCl, KCl, BaCl₂, ZnSO₄, MgCl₂, and AlCl₃ compounds, respectively, in Milli-Q water with a resistivity larger than 18 MΩ cm. Each sample solution was 10 mL. The entire experiment employed deionized water. The reagents and materials were used as received without further purification.

2.2. Fabrication of CdS thin film by AACVD method

A CdS thin film was prepared on an ITO glass substrate (1 cm × 1.5 cm) using an in-house AACVD assembly process. The synthesis strategy was reported earlier by our group [22, 23]. The ITO glass was ultrasonically cleaned in acetone, ethanol, and deionized water before being used. Then, the CdS films were prepared from 0.05 M Cd(CH₃COO)₂·2H₂O and 0.1 M CH₄N₂S in 35 mL of a methanol solution that was generated into an aerosol to be deposited as CdS on the ITO in the reaction chamber.

2.3. Fabrication of photoelectrochemical sensor electrode

The deposition of 0.1 M GO, which was produced using a simplified Hummer's method [24] on the surface of the AACVD-prepared CdS thin film was carried out using a dip-coating method, as reported by our group [22]. The CdS-GO thin film was placed in a furnace at

150°C, and argon gas was flowed for 15 min at a flow rate of 50 mL/min for the reduction process. The electrode was labeled as CdS-rGO.

2.4. Characterization techniques

The surface morphologies of the nanocomposites were analyzed using a field emission scanning electron microscope (FESEM, FEI Quanta SEM Model 400 F) equipped with an energy dispersive X-ray (EDX) accessory. The crystalline phase of the CdS-rGO nanocomposite was studied using a Philips X'pert system X-ray powder diffractometer with Cu K α radiation ($\lambda = 1.5418 \text{ \AA}$), and a Raman spectral analysis was carried out using a Renishaw inVia Raman microscope with laser excitation at $\lambda = 514 \text{ nm}$.

2.5. Photoelectrochemical studies

Photoelectrochemical measurements were performed using a homemade photoelectrochemical system containing a 150-W halogen lamp (Halooid) as the illumination source. The photocurrent signal was measured on a computer-controlled Versa-STAT-3 electrochemical analyzer from Princeton Applied Research. A CdS-rGO-modified photoelectrode with an active area of 1 cm^2 was used as the working electrode, and a Pt wire and saturated Ag/AgCl were used as the counter and reference electrodes, respectively. The working electrode potentials stated in this paper are with reference to the Ag/AgCl, unless otherwise stated. All the photocurrent measurements were conducted by dipping the CdS-rGO-modified photoelectrode into a mixture of 0.1 M KCl and 0.5 M TEA at a constant potential of 0 V vs. Ag/AgCl.

3. Results and Discussion

3.1. Morphological studies

[Fig 1\(A\)](#) shows a low-magnification FESEM image of the CdS obtained using the AACVD method at 400°C for 180 min. This image indicates that the sphere-like morphology of pure CdS was composed of homogenous nanospheres with a narrow diameter distribution of about 350–400 nm. These nanospheres were dispersed with good monodispersity ([Fig 1\(A\), inset](#)), although a few seemed to agglomerate. Upon the addition of 0.1 mg/ml GO, a transparent ultrathin GO layer was clearly observed on the surface of the CdS nanoparticles ([Fig 1\(B\)](#)). The GO nanosheets were curled and corrugated, and CdS nanospheres were distributed over the GO sheets. The GO was then reduced by sintering at a temperature and pressure of 150°C and 50 mL/min, respectively. [Fig 1\(C\)](#) shows that the rGO formed a continuous network with CdS nanoparticles, resulting in excellent hybridization of the rGO and CdS. The rGO sheets blanketed the CdS nanoparticles, which enhanced the photo-generated carriers separation, and consequently elevated the PEC performance [25]. The corresponding histograms of the particle size distribution ([Fig 1\(D\)](#)) are also shown, along with the FESEM images. The size distribution was determined based on the measurement of 180 CdS nanospheres. It is worth noting that aggregates consisting of small particles were not taken into account in the determination of the particle crystal size. It was found that most of the particles had sizes of <400 nm, and the average particle size was 350–400 nm, as indicated in the histogram.

3.2. X-ray diffraction analysis

XRD patterns revealed the effect of the graphene on the crystallinity of the CdS nanoparticles for the GO, CdS, and CdS-rGO films. Their diffraction patterns are given in [Fig 2](#). The XRD pattern of GO portrays a distinguishable peak at $2\theta = 10.6^\circ$ at the index of (002). The characteristic peaks at 245° , 26.7° , 26.8° , 30.3° , 35.2° , 43.5° , 50.6° , 51.9° , and 60.2° respectively

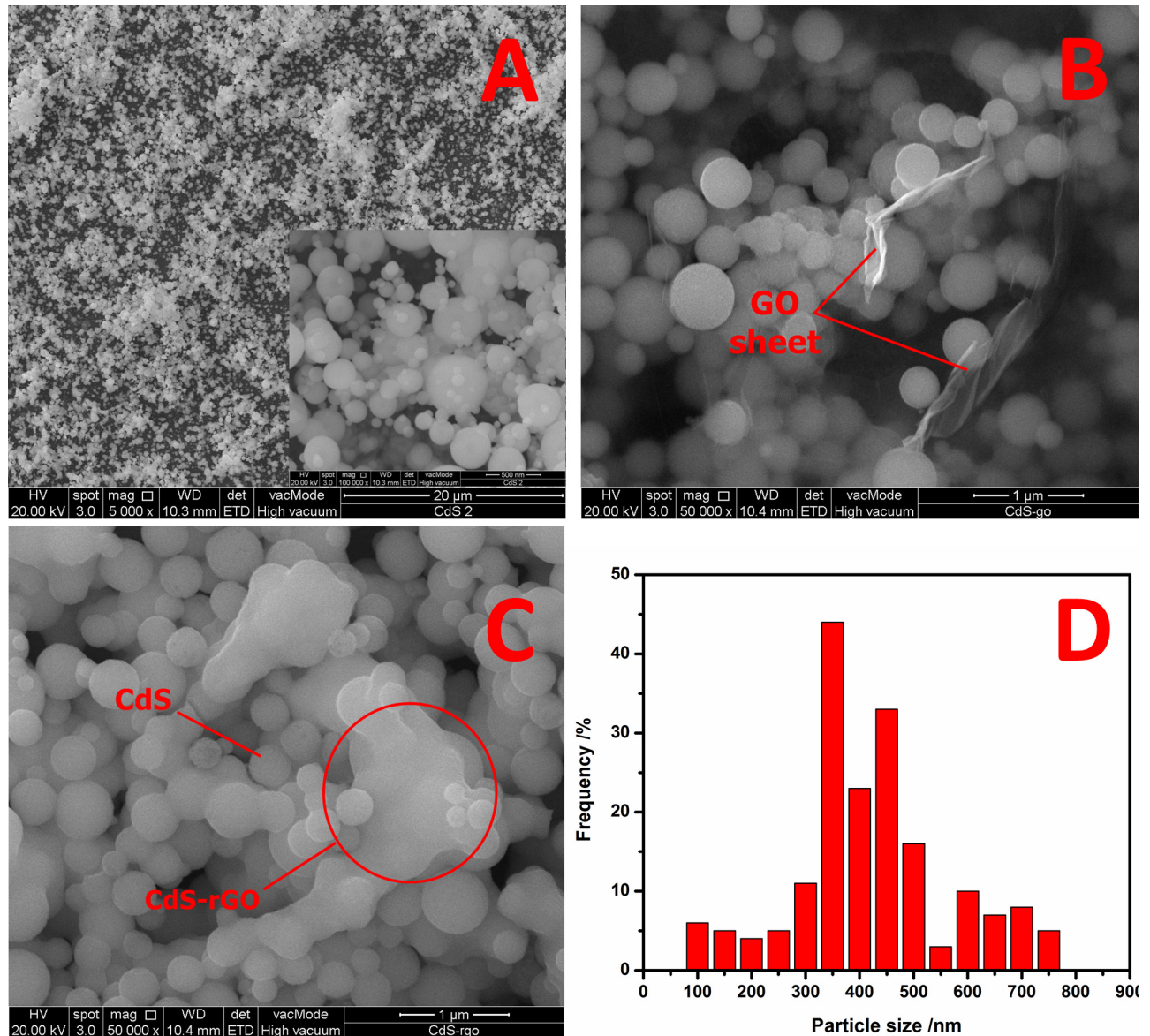


Fig 1. FESEM images of (A) CdS nanospheres, (B) CdS-GO, and (C) CdS-rGO, as well as (D) histogram showing size distribution of CdS nanoparticles in CdS-rGO nanocomposite.

doi:10.1371/journal.pone.0154557.g001

correspond to the (100), (002), (111), (101) (102), (110), (201), (112), and (202) planes of the hexagonal crystal structure of CdS (JCPDS card no.: 02–0549). The XRD pattern of the CdS-rGO nanocomposite only shows the peaks for the hexagonal CdS phase. However, the nanocomposite shows a peak with lower intensities than those for pure CdS. This would be caused by the graphene wrapped around the surface of the CdS particles, which could induce crystal diffraction. Moreover, no obvious peak is observed at the (002) index for the CdS-rGO composite, which corresponds to the oxygen-containing functional groups located between the layers of GO, suggesting that the GO was reduced to rGO during the heating treatment, and the interlayer spacing was decreased [26].

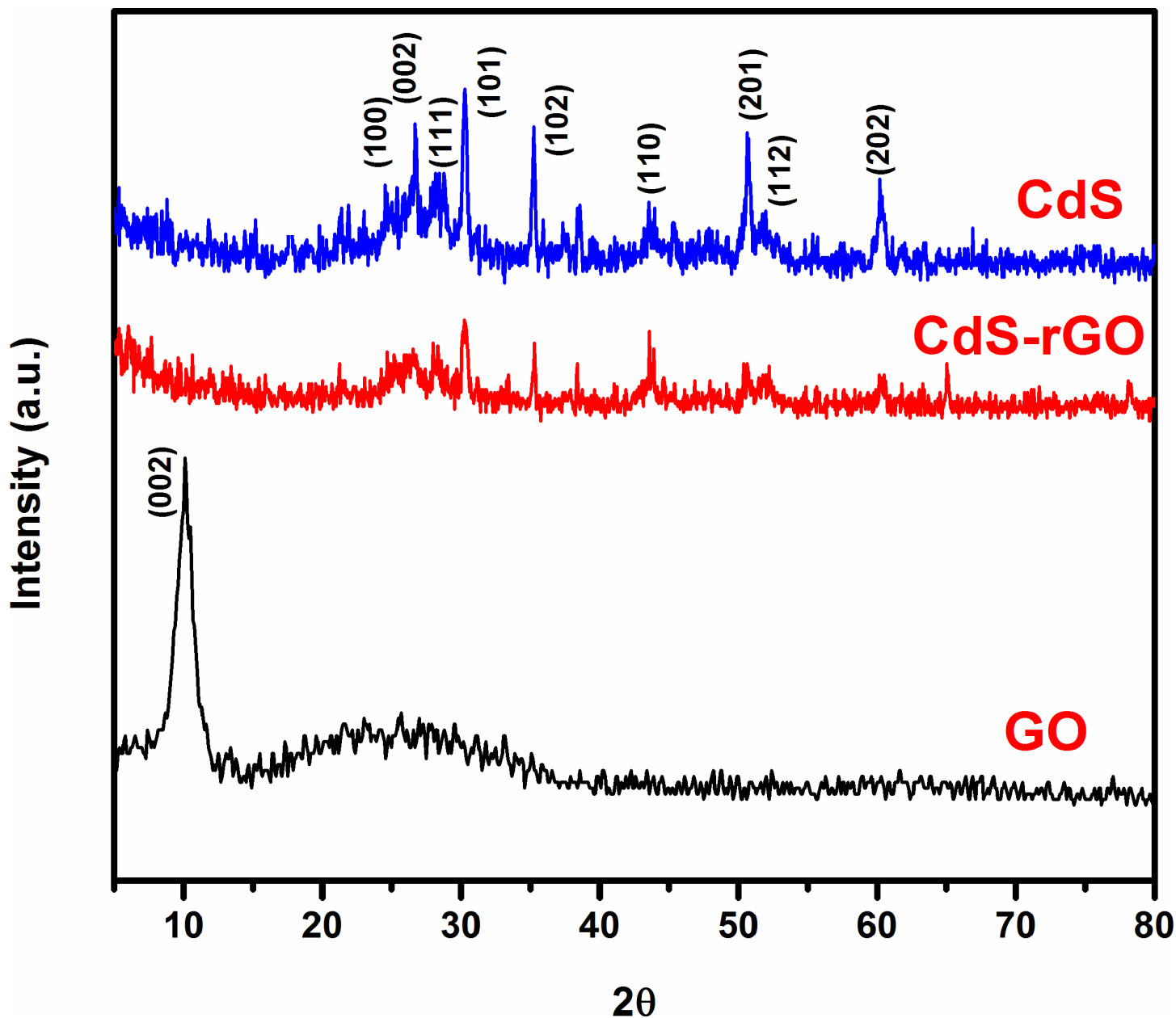


Fig 2. XRD patterns of as-prepared GO, CdS, and CdS-rGO samples.

doi:10.1371/journal.pone.0154557.g002

3.3. Raman spectral analysis

Raman spectroscopy was performed on the GO, rGO, CdS, CdS-GO, and CdS-rGO nanocomposites, and the results are shown in Fig 3. The Raman profile of GO the typical D and G bands assigned to the κ -point phonons of the A_{1g} symmetry and E_{2g} phonon of the sp^2 carbon at 1353 and 1593 cm^{-1} , respectively. These two bands shifted to lower wavenumbers of 1340 and 1577 cm^{-1} after the reduction. The chemical reduction of GO enhanced the intensity ratio of the D to G bands (I_D/I_G) from 0.974 to 0.986. The increase in the I_D/I_G ratio for rGO was due to the restoration of the sp^2 network and the formation of unrepaired defects after the removal of numerous oxygen functionalities [27, 28]. Hence, it gives a clear indication of the effective

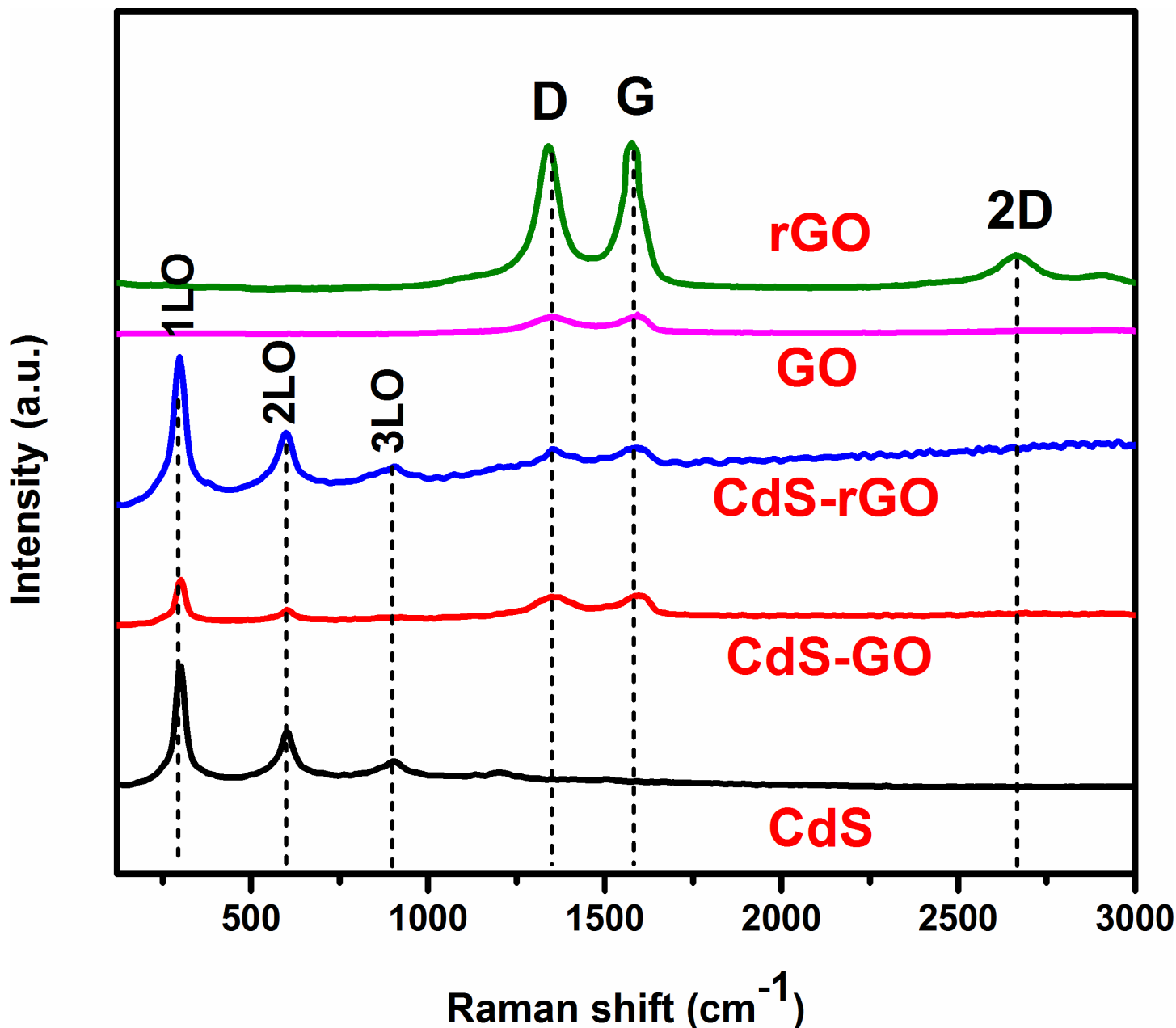


Fig 3. Raman spectra of GO, rGO, CdS, CdS-GO, and CdS-rGO.

doi:10.1371/journal.pone.0154557.g003

reduction of GO. Furthermore, the appearance of the 2D band at 2662 cm^{-1} in the rGO spectrum indicates the reduction of GO to rGO [27]. The characteristic peaks of CdS presented at 301 , 599 , and 905 cm^{-1} correspond to the first-, second-, and third-order longitudinal optical phonon modes (1LO, 2LO, and 3LO), respectively. For the CdS-rGO nanocomposite, all the Raman bands for CdS and rGO can be found. When CdS nanoparticles are deposited on graphene, the intensity of the D band increases relative to the G band, and both bands shift to higher wavenumbers [29]. In the present study, the D and G bands for the CdS/rGO composite appeared at 1355 and 1593 cm^{-1} , respectively. The intensity ratios of the D and G bands for CdS-GO and CdS-rGO were 0.989 and 0.991 , respectively. The I_D/I_G ratios for these two

nanocomposites were higher than those for GO, indicating that a significant number of structural defects were introduced to the graphene lattice in the reaction. Conclusively, the larger I_D/I_G ratios in the composite materials compared to GO indicate an increase in the amount of smaller sp^2 domains and the revival of graphene network conjugation (re-aromatization) [30]. Moreover, the revived graphene network size was smaller than that of the GO starting material. This effect gave rise to an increased I_D/I_G ratio in the CdS/rGO composite materials [31].

3.4. Electrochemical impedance spectroscopy analysis

The electron transfer characteristics and recombination processes at the electrolyte and electrode interfacial surface were investigated using the electrochemical impedance spectra (EIS) in 0.1 M KCl and 0.5 M TEA, as shown by Nyquist plots (Fig 4). The EIS were found in a frequency range of 10 kHz to 0.01 Hz to evaluate the frequency response of the nanocomposites.

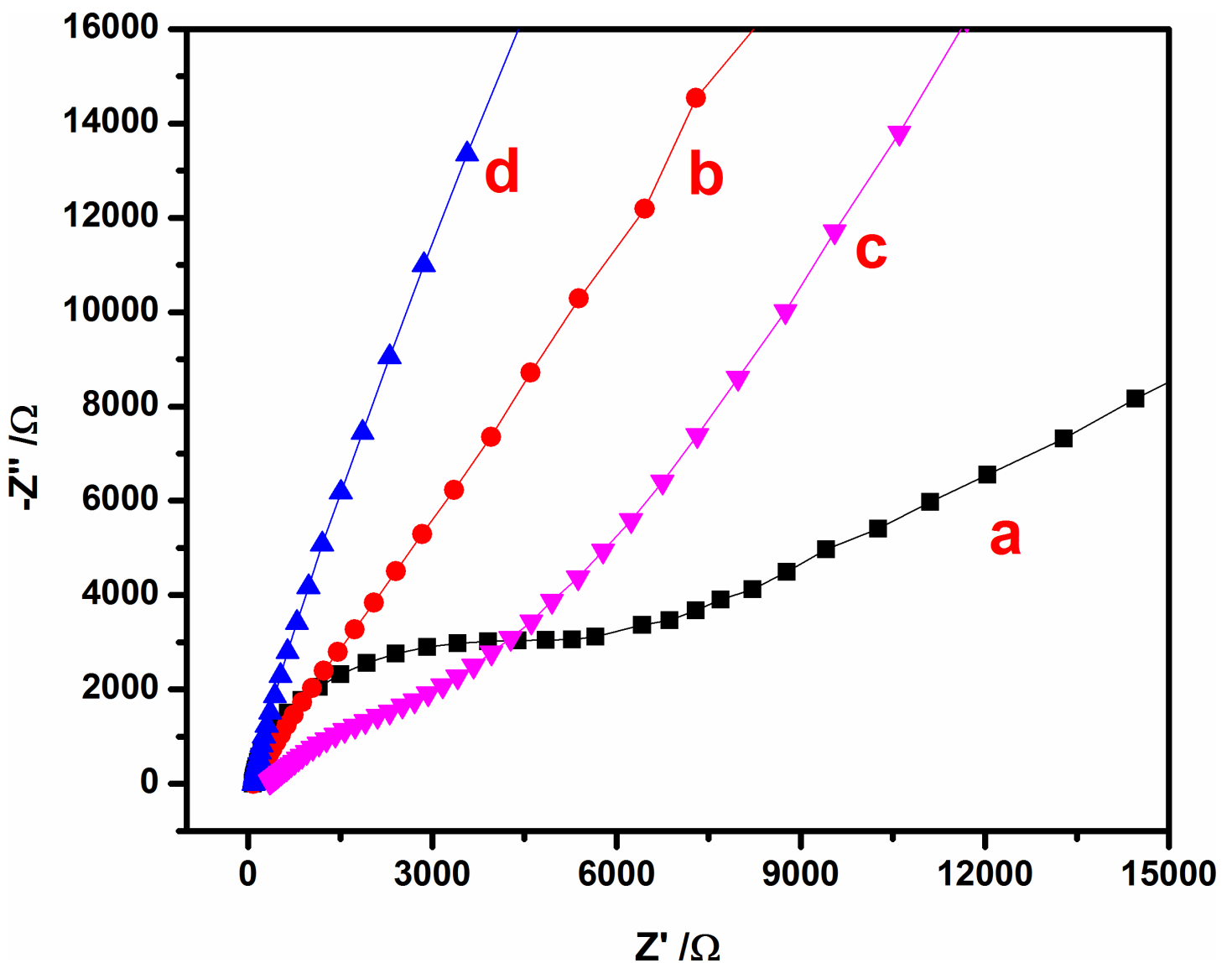


Fig 4. Nyquist plots obtained for (a) CdS, (b) CdS-GO, (c) CdS-rGO, and (d) CdS-rGO-Cu after addition of 4 μM Cu²⁺ ions into 0.1 M KCl and 0.5 M TEA solution.

doi:10.1371/journal.pone.0154557.g004

The equivalent series resistance (ESR) was extracted from the x-intercept of the Nyquist plot to evaluate the resistance of the KCl and TEA mixture solution, intrinsic resistance of the nanocomposite, and contact resistance at the interface between the electrode and current collector [32, 33]. The ESR values for the CdS, CdS-GO, CdS-rGO, and CdS-rGO-Cu were 89.14, 88.24, 72.37, and 351.22 Ω , respectively. The CdS-rGO electrode (Fig 4, curve c) shows a lower resistance value, indicating that the presence of rGO improved the transfer of the charge performance of the CdS electrode. Meanwhile, the larger resistance value of the CdS-rGO-Cu electrode (curve d) was due to the presence of Cu²⁺ ions on the CdS-rGO electrode, which hindered the electron transfer to the as-prepared electrode, increasing the intrinsic resistance of the nanocomposite. In the high-frequency range, the sizable semi-circle indicates the high charge transfer resistance (R_{ct}) caused by the weak transfer of the generated electrons and the recombination properties [10]. In the Nyquist plots, CdS-rGO exhibits a smaller semi-circle of 10.85 Ω compared to CdS-GO (25.33 Ω), suggesting that the electrochemically unstable oxygenous groups were removed during the reduction, hence overcoming the pseudocapacitance [34]. The CdS-GO (curve b) appears to have a large R_{ct} because of excessive oxygenated species, which produced an insulating behavior and obstructed its electrochemical characteristics [35]. Obviously, bare CdS electrodes (curve c) appear to have the largest semi-circle of 8841.2 Ω , particularly because of the absence of rGO, which behaved as an electron transfer medium for CdS excitation [36]. The CdS-rGO-Cu shows a slightly high R_{ct} value of 7700.4 Ω , demonstrating that the Cu²⁺ ions were successfully incorporated on the surface of the sensor electrode [36], which provided a sensitive sensing platform for Cu²⁺ ion detection. Additionally, the low-frequency region portrays a straight line caused by a diffusion-limiting process that is more vertical for CdS-rGO, implying even more diffusion routes for electrons within the CdS-rGO electrode [34], and hence rapid electrolyte diffusion on the electrode-electrolyte interfaces [37].

3.5. Photoelectrochemical performance

S1(A) Fig shows the linear sweeps of the CdS-rGO electrode in a potential range of -0.6 to 1.0 V versus Ag/AgCl in 0.1 M KCl electrolyte. Under irradiation, the CdS-rGO electrode achieved a maximal current of 100.07 μ A at an applied bias of 0.96 V versus Ag/AgCl. Meanwhile, the current was obviously low in the absence of light irradiation, and it had a maximum current of 89.87 μ A. The light alternated in 30-s intervals (light on and off) showed the comparable and instantaneous photocurrent response under light and dark conditions due to the PEC effect [38]. Likewise, **S1(B) Fig** appears to have a similar LSV to that in **S1(A) Fig** but the photocurrent response for **S1(B) Fig** is much more pronounced. The current response upon light illumination was 163.03 μ A at 0.70 V versus Ag/AgCl, while in the dark condition, it had a current response of 140.47 μ A with the same applied bias. The enhanced photocurrent was due to the introduction of 0.5 M TEA in the electrolyte. This is because TEA is a suitable sacrificial electron donor, leading to rapid electron-hole separation, and thus magnifying the photoelectrochemical responses and minimizing the over potential [39]. Conclusively, the CdS-rGO electrode worked extremely well in the presence of TEA, thus giving a stronger current response because more electrons were brought together from the PEC reaction, which suggests an improved separation efficiency [40]. Upon the addition of 4 μ M of Cu²⁺ ions, the photocurrent dropped even more dramatically (**S1(C) Fig**). The current was reduced to 67.41 μ M under light irradiation and 44.96 μ M in the dark condition, both at an applied bias of 0.60 V versus Ag/AgCl. The photocurrent decrease corresponded to the extensive carrier recombination rate [41]. The obvious increase in cathodic current at potentials of -0.20 to -0.10 V was a result of the reduction in Cu²⁺ ions, corresponding to the following reaction: $\text{Cu}^{2+} + e^{-} \rightarrow \text{Cu}^{+}$. Further,

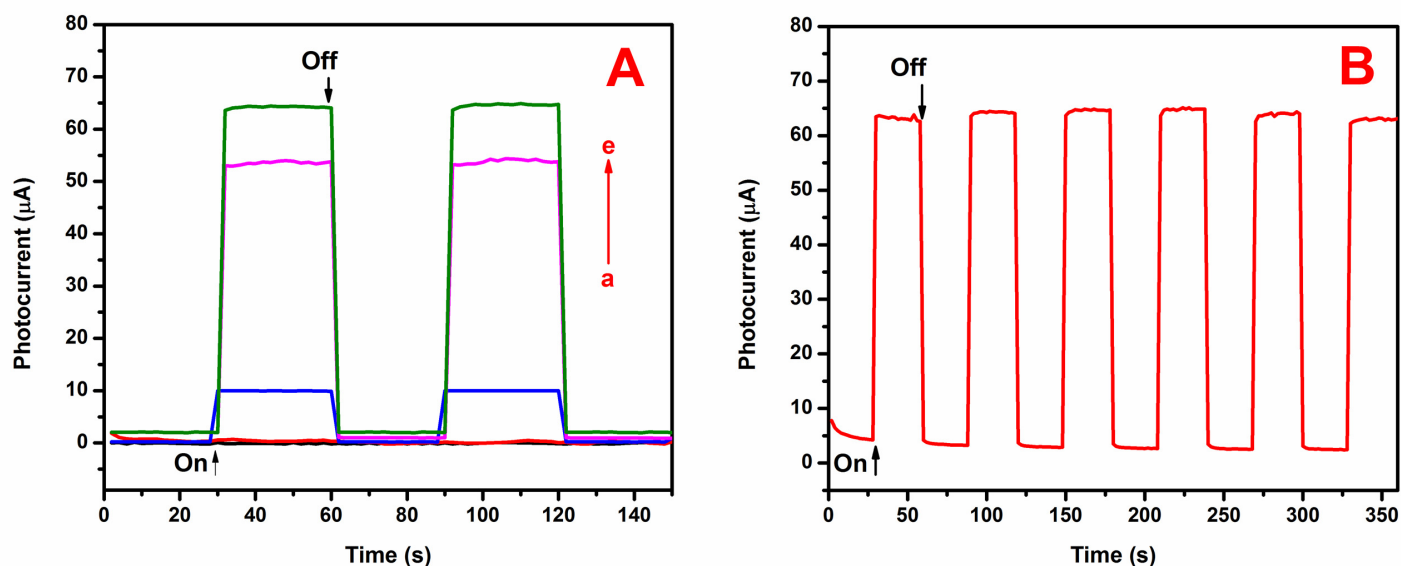


Fig 5. (A) Photocurrent responses of (a) rGO-, (b) GO-, (c) CdS-, (d) CdS-GO-, and (e) CdS-rGO-modified electrodes and (B) time-based photocurrent response of ITO/CdS-rGO in 0.1 M KCl and 0.5 M TEA under chopped irradiation.

doi:10.1371/journal.pone.0154557.g005

the influence of the photocurrent performance was investigated in the absence and presence of 4 μM Cu²⁺ ions with 0.1 M KCl and 0.5 M TEA under the light “on-off” condition (S1(D) Fig). It was clear for both the absence and presence of Cu²⁺ ions that the current was higher under light illumination and declined when the light was cut off. Upon the addition of Cu²⁺ ions into the solution, there was a reduction in the photocurrent compared to the former value. This suggests that the photocurrent quenching was due to the photocatalytic reduction of Cu²⁺ to Cu⁺ ions. From the results obtained, the photocurrent increased as the electrode potential was made more positive, suggesting that an anodic photocurrent appeared, with electrons as its majority carriers [42]. Thus, the ITO/CdS-rGO electrode behaved as an n-type semiconductor electrode. The n-type material induced oxidation on the electrolyte species at the semiconductor-electrolyte during the PEC performance [42].

Subsequently, the PEC response was investigated by employing different materials to decorate the ITO sheet used as a photoanode. The photocurrent of each prepared sample was calculated in a 0.1 M KCl solution containing 0.1 M TEA under “on-off” light illumination cycles at a bias of 0 V vs. Ag/AgCl, as shown in Fig 5(A). The photoresponse for rGO was non-existent because rGO could not be excited, as shown in curve a [43]. Similarly, for GO (curve b), no obvious photocurrent was observed. This was typically due to the nature of graphene oxide, which is electrically insulating and requires further reduction steps to generate a photocurrent signal [44]. After modification by the AACVD process, the ITO/CdS electrode increased the photocurrent to 9.96 μA (curve c). For the ITO/CdS-rGO electrode, this could boost the photocurrent by at least 6-fold, reaching a value of 64.35 μA (curve e). CdS nanoparticles were bound to the surface of the rGO nanosheets through the van der Waals force [45]. The binding force enabled the CdS nanoparticles to integrate intimately with the ITO electrode. The encapsulation of CdS by the rGO improved the interfacial contact, which facilitated the electron transfer between the CdS and ITO, thus preventing possible current leakage in the ITO/CdS-rGO electrode. Besides, rGO is also capable of dividing and accumulating the photogenerated electrons, which minimizes the recombination rate of the photogenerated electrons and holes, and boosts

the photocurrent production [46, 47]. Meanwhile, for the ITO/CdS-GO electrode (curve d), a slightly lower signal (16.27% or 53.88 μA) was revealed compared to CdS-rGO. This was because the electrical conductivity of rGO is higher than that of GO [48].

The stability of the amperometric response of the CdS-rGO-modified photoelectrode in the presence of 0.5 M TEA under the light “on-off” condition is given in Fig 5(B). This graph displays the photocurrent response of the ITO/CdS-rGO based on time, which was repeatedly measured six times at 30-s intervals under visible irradiation. No current was observed in the dark, which clearly suggests that no photoinduced charge separation took place. Interestingly, when the light was turned on, the photocurrent intensity was significantly increased to 64.35 μA . This may have been due to the photoinduced electron-hole separation at the CdS, in which the holes were scavenged by the TEA, and rGO acted as an electron transfer medium. Thus, the electrons were transported to the ITO electrode, resulting in photocurrent generation. The electrode showed a pronounced and stable photocurrent response during the light “on-off” condition, which it maintained. The relative standard deviation was only 1.02%, which implied that the constructed PEC sensor had a stable photocurrent activity.

3.6. Photoelectrochemical detection of copper(II) ions

As shown in Fig 6(A), the PEC performance of the CdS-rGO was evaluated by the sensing of Cu²⁺ ions. The photocurrent density of the ITO/CdS-rGO decreased with increasing concentration of Cu²⁺ ions. Fig 6(B) shows the increase in the photocurrent ΔI ($\Delta I = I - I_0$) and the Cu²⁺ ions concentration, where I and I_0 are the photocurrent intensities of CdS-rGO in the presence and absence of Cu²⁺ ions, respectively. The inset of Fig 6(B) shows an excellent linear relationship of $R^2 = 0.9915$. The regression equation was ΔI (μA) = 13.89 + 6.97 log [Cu²⁺] (μM) between the value of ΔI and the logarithm of the Cu²⁺ ions concentration of 0.5–120.0 μM . The limit of detection (LoD) was evaluated using $3\sigma/S$ and was found to be 0.016 μM , where σ is the standard deviation of a blank signal, and S is the slope of the linear calibration plot. A possible schematic mechanism for the PEC discernment of Cu²⁺ ions is shown in Fig 7. Under illumination, the photogenerated electrons are transferred from the valence band (VB) to the conduction band (CB) of a CdS nanoparticles present in the CdS-rGO nanocomposite, and then holes are generated in the VB. The photogenerated holes are scavenged by TEA, and the electrons are promoted to the CB of CdS. Hence, when CdS was in contact with graphene, the photogenerated electrons in the CB of the CdS were transferred to the two-dimensional carbon sheets, which hindered the charge recombination and prolonged the lifetime of the photogenerated carriers. The photocurrent intensity was greatly decreased upon the addition of Cu²⁺ ions. The addition of Cu²⁺ ions to CdS resulted in the binding of Cu²⁺ with S²⁻, and the reduction of Cu²⁺ to Cu⁺ ions under irradiation. Consequently, Cu_xS ($x = 1, 2$) was formed on the surface of CdS because Cu²⁺ chemically displaced Cd²⁺ because Cu_xS has a lower solubility than CdS. The development of recombination centers (Cu_xS) on the CdS surface generated a low band gap energy, which effectively recombined excited electrons in the CB and holes in the VB [49–52]. In addition, to prove the quenching of the photocurrent upon the addition of Cu²⁺ ions, FESEM images were recorded for the CdS-rGO nanocomposite after the addition of Cu²⁺ ions to the photoelectrochemical cell. In Fig 6(C), a small hole is observed in some of the spherical CdS structures due to the presence of 1.15% Cu content in the CdS-rGO nanocomposite. The transparent ultrathin rGO sheets were seen to retain their role of linking the spherical CdS, even after the addition of 4 μM Cu²⁺ ions under an illuminated condition. A comparison of this FESEM image with Fig 6(B) clearly indicates a photocurrent quenching due to the formation of Cu_xS, *i.e.*, analyte-induced morphological changes caused by photocurrent quenching. The presence of CdS in the composite was demonstrated

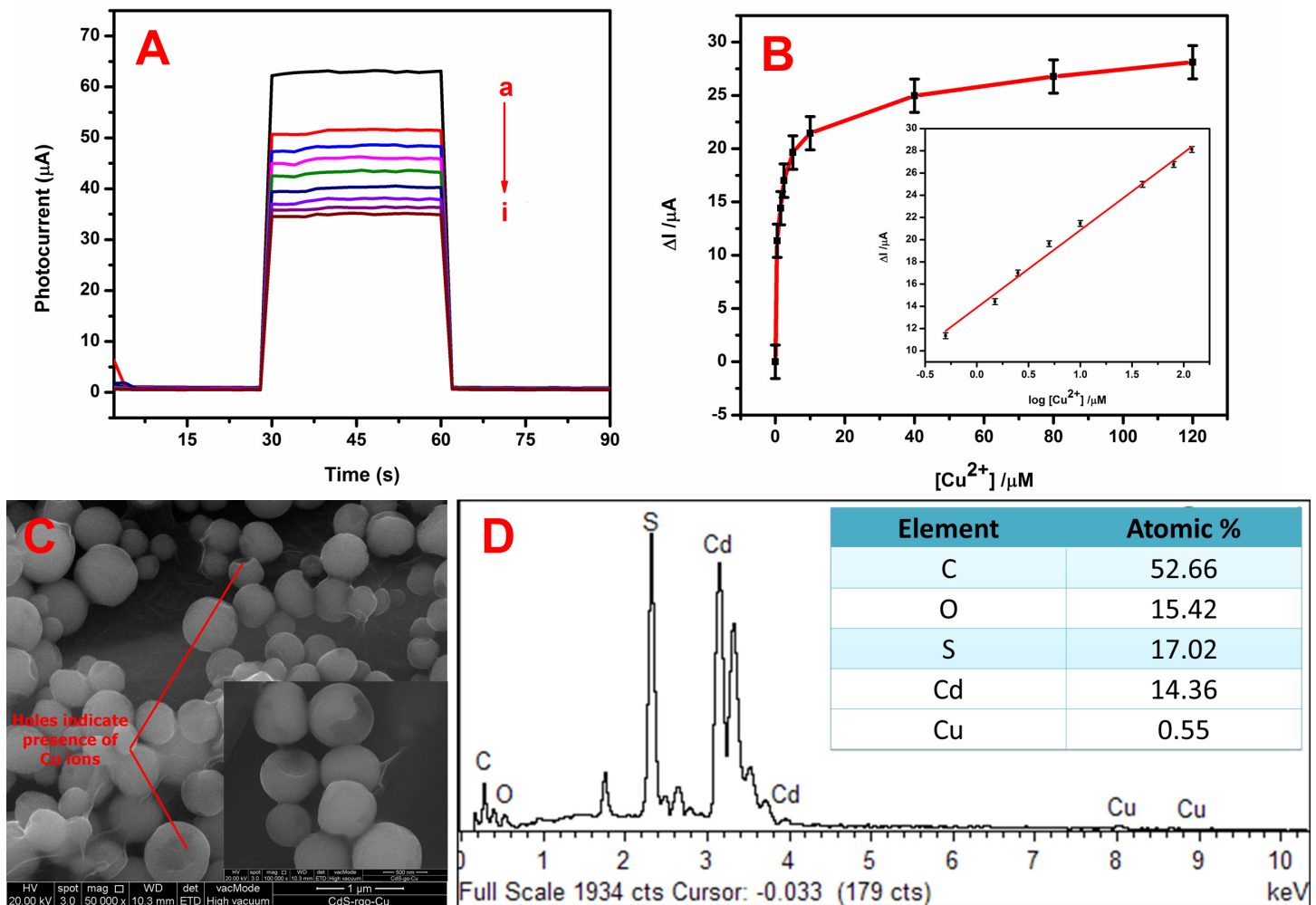


Fig 6. (A) Photocurrent responses of ITO/CdS-rGO electrode at different concentrations of Cu²⁺ ions: (a) 0, (b) 0.5, (c) 1.5, (d) 2.5, (e) 5.0, (f) 10.0 (g) 40.0, (h) 80.0, and (i) 120 μM, and (B) photocurrent change against Cu²⁺ ions concentration. Inset: corresponding calibration curve. (C) Low-magnification image of CdS-rGO-Cu, inset: high-magnification image of CdS-rGO-Cu, and (D) EDX spectrum of CdS-rGO-Cu, inset: weight percentage of elements found in spectrum.

doi:10.1371/journal.pone.0154557.g006

by the Cd and S peaks in the EDX profile (Fig 6(D)). The spectrum reveals an atomic Cd to S ratio of about 1:1, which agrees with the stoichiometric CdS. The C came from graphene, and the O was contributed by the residual oxygenous groups on the rGO. Thus, the result indicates

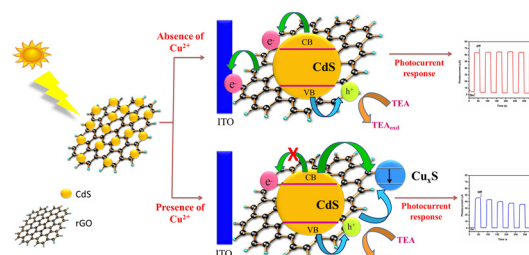


Fig 7. Mechanism for sensing Cu²⁺ ions based on ITO/CdS-rGO nanocomposites.

doi:10.1371/journal.pone.0154557.g007

Table 1. Comparison of various Cu²⁺ ions sensor based on various detection methods.

Detection method	Electrode/substrate	Electrode preparation	Linear range (μM)	LoD (μM)	Ref.
Photoelectrochemical sensor	Cd _x Zn _{1-x} S-rGO on GCE	facile one-pot reaction	0.02–20	0.067	[46]
Photoelectrochemical sensor	SnO ₂ /CdS heterostructural films on FTO	SILAR	1.0–38.0	0.55	[11]
Electrochemiluminescence	MPA-capped CdTe/CdS	In-situ	0.1–10	0.02	[53]
Luminescent chemosensor	CdS cluster, [Cd ₁₀ S ₄ (SR) ₁₂]	Ligand-exchange reaction	10	0.07	[54]
Luminescent response	L-cysteine and thioglycerol-capped CdS QD	Reflux	1600	1	[50]
Fluorescence resonance energy transfer (FRET)	Phenol formaldehyde resin PFR-CdTe QDs	Hydrothermal	0.80–5.36	0.16	[55]
Adsorption stripping voltametry (AdSV)	CPE modified with Ac-Phos SAMMS	Adsorption of monolayers	0.160–3.147	0.0786	[56]
Potentiometric method using ion-selective electrodes	CPE modified with MWCNT	In-situ	0.01–10000	1.07	[57]
Differential pulse voltammetry measurement	Carbon tip electrode modified with mercury film	Electrochemical deposition	9.44–157.37	1.57	[58]
Photoelectrochemical sensor	CdS-rGO on ITO	AACVD	0.5–120	0.016	Present work

doi:10.1371/journal.pone.0154557.t001

that the CdS was successfully deposited on the rGO sheets. In contrast, the small peak observed in the EDX spectrum implies the existence of 0.55 atomic % of Cu²⁺ (Fig 6(D), inset). Therefore, the photocurrent intensity of the CdS-rGO decreased in the Cu²⁺ ion solution, making the nanocomposite suitable for the selective determination of Cu²⁺ ions.

Even though much research has been reported on the PEC sensing of Cu²⁺ ions, our current work demonstrated a facile, environmentally friendly, and low-cost method, especially in relation to the synthesis of a modified electrode. There has been no work reported based on the AACVD synthesis of CdS using cadmium acetate and thiourea as the precursors. In addition, an ITO/CdS-rGO electrode holds the promise of high sensitivity toward Cu²⁺ ions, without requiring a ternary hybrid such as Cd_xZn_{1-x}S-rGO [46] and MPA-capped CdTe/CdS [53]. Some of the Cu²⁺ ions sensors with various detection methods are presented in Table 1. As shown in Table 1, the LoD obtained from the ITO/CdS-rGO-modified electrode was the lowest compared to the other reported works. Our LoD of 0.016 μM is far below the WHO's guideline value of ~20 μM that is allowed for Cu²⁺ ions in drinking water. This indicates that the proposed PEC sensor is ultra-sensitive and holds promise for the detection of a trace amount of Cu²⁺ ions in drinking water.

3.7. Interference studies

The selectivity of a Cu²⁺ ions assay was determined by investigating the influences of various kinds of metal ions at the same concentration of 120 μM, including Ni²⁺, Co²⁺, Fe³⁺, Mn²⁺, Na⁺, K⁺, Ba²⁺, Zn²⁺, Mg²⁺, and Al³⁺, on the photocurrent response of the prepared ITO/CdS-rGO electrode when the concentration of Cu²⁺ ions was at 0.5 μM. As shown in Fig 8, even with a 240-fold excess of another metal ion (120 μM vs. 0.5 μM Cu²⁺ ions), no significant photocurrent change can be seen in comparison with Cu²⁺ ions. In addition, it was observed that the photocurrent intensity of the ITO/CdS-rGO electrode was also decreased by Ni²⁺, Co²⁺, Fe³⁺, Na⁺, Zn²⁺, Mg²⁺, and Al³⁺. This was due to the displacement of Cd²⁺, leading to the formation of MS (for M = Ni, Co, Fe, Na, Zn, Mg, Al) on the CdS surface [31]. The formed MS behaved as sites for recombining photogenerated electron-hole pairs due to its defects on the

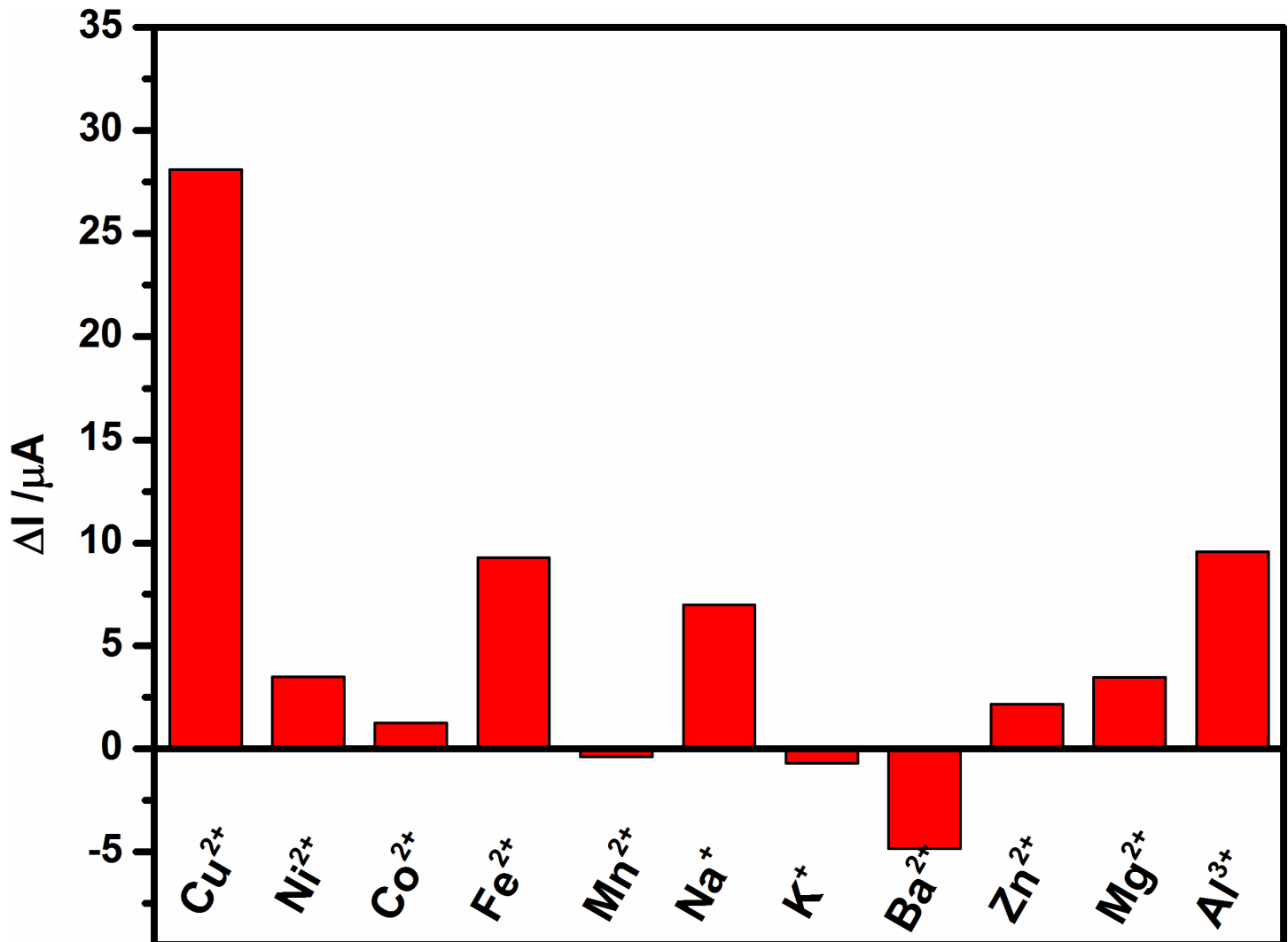


Fig 8. Photocurrent changes in prepared ITO/CdS-rGO electrode toward 0.5 μM Cu²⁺ ions against 120 μM of other metal ions.

doi:10.1371/journal.pone.0154557.g008

surface and lower band energy. However, the ITO/CdS-rGO electrode was significantly sensitive to Cu²⁺ ions compared to the other metal ions because CuS has a notably lower K_{sp} value than NiS, CoS, FeS, and ZnS [31]. Hence, the prepared ITO/CdS-rGO electrode was sensitive and selective toward Cu²⁺ ions.

Conclusion

A PEC sensor based on the CdS-rGO nanocomposite was successfully fabricated using AACVD and dip-coating strategies. The CdS-rGO nanocomposite showed the highest PEC activity compared to that of bare GO, rGO, CdS, and CdS-GO electrodes under visible-light illumination. This was because the presence of rGO facilitated the transfer of electrons from the conduction band of the CdS, thus manifesting the photocurrent performance of the nanocomposite. The photocurrent intensity of the CdS-rGO nanocomposite was effectively suppressed by the displacement of Cd²⁺ by Cu²⁺. This phenomenon resulted in a PEC sensor with

heightened sensitivity and selectivity toward Cu²⁺ ions, manifesting its potential in real applications.

Supporting Information

S1 Fig. LSV obtained for ITO/CdS-rGO photoelectrode dipped into (A) 0.1 M KCl, (B) mixture of 0.1 M KCl and 0.5 M TEA, and (C) 0.1 M KCl, 0.5 M TEA, and 4 μM Cu (II) under (a) light irradiation, (b) dark condition, and (c) light “on-off” condition. (D) LSV responses in (a) absence and (b) presence of 4 μM Cu²⁺ ions with 0.1 M KCl and 0.5 M TEA under light “on-off” condition at scan rate of 0.1 Vs⁻¹. (DOCX)

Acknowledgments

This research work was supported by a Wighton Titular Fellowship in Engineering (6385600–10501) and a High Impact Research Grant (UM.C/625/1/HIR/MOHE/SC/21) from the Ministry of Higher Education.

Author Contributions

Conceived and designed the experiments: II HNL NMH AP. Performed the experiments: II. Analyzed the data: II HNL. Contributed reagents/materials/analysis tools: HNL NMH. Wrote the paper: II HNL. Designed the homemade PEC system and experimental method: II HNL NMH AP. Gave an idea and advice on every problem that occurred while doing this research: II HNL NMH AP. Gave ideas on Cu²⁺ metal ion sensing: II HNL NMH AP. Contribution on research fund: HNL NMH.

References

1. Trumbo P, Yates AA, Schlicker S, Poos M. Dietary reference intakes: vitamin A, vitamin K, arsenic, boron, chromium, copper, iodine, iron, manganese, molybdenum, nickel, silicon, vanadium, and zinc. *Journal of the American Dietetic Association*. 2001; 101(3):294–301. PMID: [11269606](#)
2. Guidelines for drinking-water quality: recommendations: World Health Organization; 1993.
3. Lan GY, Huang CC, Chang HT. Silver nanoclusters as fluorescent probes for selective and sensitive detection of copper ions. *Chemical Communications*. 2010; 46(8):1257–9. doi: [10.1039/b920783j](#) PMID: [20449269](#)
4. Lee SH, Sumranjit J, Tongkate P, Chung BH, Lee HJ. Voltammetric Studies of Cu (II) Ion Transfer Reaction with Picolinamide-phenylenevinylene across Liquid/Liquid Interfaces and Their Sensing Applications. *Electrochimica Acta*. 2014; 123:198–204.
5. Li H, Hao W, Hu J, Wu H. A photoelectrochemical sensor based on nickel hydroxyl-oxide modified n-silicon electrode for hydrogen peroxide detection in an alkaline solution. *Biosensors and Bioelectronics*. 2013; 47:225–30. doi: [10.1016/j.bios.2013.03.028](#) PMID: [23584227](#)
6. Wang P, Dai W, Ge L, Yan M, Ge S, Yu J. Visible light photoelectrochemical sensor based on Au nanoparticles and molecularly imprinted poly (o-phenylenediamine)-modified TiO₂ nanotubes for specific and sensitive detection chlorpyrifos. *Analyst*. 2013; 138(3):939–45. doi: [10.1039/c2an36266j](#) PMID: [23232561](#)
7. Lu W, Jin Y, Wang G, Chen D, Li J. Enhanced photoelectrochemical method for linear DNA hybridization detection using Au-nanoparticle labeled DNA as probe onto titanium dioxide electrode. *Biosensors and Bioelectronics*. 2008; 23(10):1534–9. doi: [10.1016/j.bios.2008.01.011](#) PMID: [18294836](#)
8. Li H, Li J, Wang W, Yang Z, Xu Q, Hu X. A subnanomole level photoelectrochemical sensing platform for hexavalent chromium based on its selective inhibition of quercetin oxidation. *Analyst*. 2013; 138(4):1167–73. doi: [10.1039/c2an36605c](#) PMID: [23282732](#)
9. Gao P, Ma H, Yang J, Wu D, Zhang Y, Du B, et al. Anatase TiO₂ based photoelectrochemical sensor for the sensitive determination of dopamine under visible light irradiation. *New Journal of Chemistry*. 2015.

10. Shen Q, Zhao X, Zhou S, Hou W, Zhu JJ. ZnO/CdS hierarchical nanospheres for photoelectrochemical sensing of Cu²⁺. *The Journal of Physical Chemistry C*. 2011; 115(36):17958–64.
11. Huang F, Pu F, Lu X, Zhang H, Xia Y, Huang W, et al. Photoelectrochemical sensing of Cu²⁺ ions with SnO₂/CdS heterostructural films. *Sensors and Actuators B: Chemical*. 2013; 183:601–7.
12. Liu S, Chen Z, Zhang N, Tang ZR, Xu YJ. An Efficient Self-Assembly of CdS Nanowires–Reduced Graphene Oxide Nanocomposites for Selective Reduction of Nitro Organics under Visible Light Irradiation. *The Journal of Physical Chemistry C*. 2013; 117(16):8251–61.
13. Pawar RC, Lee CS. Single-step sensitization of reduced graphene oxide sheets and CdS nanoparticles on ZnO nanorods as visible-light photocatalysts. *Applied Catalysis B: Environmental*. 2014; 144:57–65.
14. Wang P, Jiang T, Zhu C, Zhai Y, Wang D, Dong S. One-step, solvothermal synthesis of graphene-CdS and graphene-ZnS quantum dot nanocomposites and their interesting photovoltaic properties. *Nano Research*. 2010; 3(11):794–9.
15. Sheeney Haj Ichia L, Basnar B, Willner I. Efficient generation of photocurrents by using CdS/carbon nanotube assemblies on electrodes. *Angewandte Chemie International Edition*. 2005; 44(1):78–83.
16. Chen D, Feng H, Li J. Graphene oxide: preparation, functionalization, and electrochemical applications. *Chemical reviews*. 2012; 112(11):6027–53. doi: [10.1021/cr300115g](https://doi.org/10.1021/cr300115g) PMID: [22889102](https://pubmed.ncbi.nlm.nih.gov/22889102/)
17. Novoselov K, Geim AK, Morozov S, Jiang D, Katsnelson M, Grigorieva I, et al. Two-dimensional gas of massless Dirac fermions in graphene. *nature*. 2005; 438(7065):197–200. PMID: [16281030](https://pubmed.ncbi.nlm.nih.gov/16281030/)
18. Balandin AA, Ghosh S, Bao W, Calizo I, Teweldebrhan D, Miao F, et al. Superior thermal conductivity of single-layer graphene. *Nano letters*. 2008; 8(3):902–7. doi: [10.1021/nl0731872](https://doi.org/10.1021/nl0731872) PMID: [18284217](https://pubmed.ncbi.nlm.nih.gov/18284217/)
19. Bunch JS, Verbridge SS, Alden JS, Van Der Zande AM, Parpia JM, Craighead HG, et al. Impermeable atomic membranes from graphene sheets. *Nano letters*. 2008; 8(8):2458–62. doi: [10.1021/nl801457b](https://doi.org/10.1021/nl801457b) PMID: [18630972](https://pubmed.ncbi.nlm.nih.gov/18630972/)
20. Allen MJ, Tung VC, Kaner RB. Honeycomb carbon: a review of graphene. *Chemical reviews*. 2009; 110(1):132–45.
21. Zhao WW, Ma ZY, Yu PP, Dong XY, Xu JJ, Chen HY. Highly sensitive photoelectrochemical immunoassay with enhanced amplification using horseradish peroxidase induced biocatalytic precipitation on a CdS quantum dots multilayer electrode. *Analytical chemistry*. 2011; 84(2):917–23. doi: [10.1021/ac203184g](https://doi.org/10.1021/ac203184g) PMID: [22148581](https://pubmed.ncbi.nlm.nih.gov/22148581/)
22. Jumeri F, Lim H, Zainal Z, Huang N, Pandikumar A. Titanium dioxide-reduced graphene oxide thin film for photoelectrochemical water splitting. *Ceramics International*. 2014; 40(9):15159–65.
23. Lim SP, Pandikumar A, Huang NM, Lim HN. Silver/titania nanocomposite-modified photoelectrodes for photoelectrocatalytic methanol oxidation. *International Journal of Hydrogen Energy*. 2014; 39(27):14720–9.
24. Huang N, Lim H, Chia C, Yarmo M, Muhamad M. Simple room-temperature preparation of high-yield large-area graphene oxide. *International journal of nanomedicine*. 2011; 6:3443. doi: [10.2147/IJN.S26812](https://doi.org/10.2147/IJN.S26812) PMID: [22267928](https://pubmed.ncbi.nlm.nih.gov/22267928/)
25. Liu X, Pan L, Lv T, Zhu G, Sun Z, Sun C. Microwave-assisted synthesis of CdS–reduced graphene oxide composites for photocatalytic reduction of Cr (vi). *Chemical Communications*. 2011; 47(43):11984–6. doi: [10.1039/c1cc14875c](https://doi.org/10.1039/c1cc14875c) PMID: [21960206](https://pubmed.ncbi.nlm.nih.gov/21960206/)
26. Wang DW, Li F, Wu ZS, Ren W, Cheng HM. Electrochemical interfacial capacitance in multilayer graphene sheets: Dependence on number of stacking layers. *Electrochemistry Communications*. 2009; 11(9):1729–32.
27. Vusa CSR, Berchmans S, Alwarappan S. Facile and green synthesis of graphene. *RSC Advances*. 2014; 4(43):22470–5.
28. Rao LG, Guns E, Rao AV. Lycopene: its role in human health and disease. *AgroFood Industry hi-tech*. 2003; 15:25–30.
29. Subrahmanyam K, Manna AK, Pati SK, Rao C. A study of graphene decorated with metal nanoparticles. *Chemical Physics Letters*. 2010; 497(1):70–5.
30. Song S, Gao W, Wang X, Li X, Liu D, Xing Y, et al. Microwave-assisted synthesis of BiOBr/graphene nanocomposites and their enhanced photocatalytic activity. *Dalton Transactions*. 2012; 41(34):10472–6. doi: [10.1039/c2dt31088k](https://doi.org/10.1039/c2dt31088k) PMID: [22825685](https://pubmed.ncbi.nlm.nih.gov/22825685/)
31. Pan S, Liu X. ZnS–graphene nanocomposite: synthesis, characterization and optical properties. *Journal of Solid State Chemistry*. 2012; 191:51–6.
32. Aravinda L, Nagaraja K, Nagaraja H, Bhat KU, Bhat BR. ZnO/carbon nanotube nanocomposite for high energy density supercapacitors. *Electrochimica Acta*. 2013; 95:119–24.
33. Haldorai Y, Voit W, Shim JJ. Nano ZnO@ reduced graphene oxide composite for high performance supercapacitor: Green synthesis in supercritical fluid. *Electrochimica Acta*. 2014; 120:65–72.

34. Yang J, Gunasekaran S. Electrochemically reduced graphene oxide sheets for use in high performance supercapacitors. *Carbon*. 2013; 51:36–44.
35. Chen Y, Zhang X, Zhang D, Yu P, Ma Y. High performance supercapacitors based on reduced graphene oxide in aqueous and ionic liquid electrolytes. *Carbon*. 2011; 49(2):573–80.
36. Sun B, Zhang K, Chen L, Guo L, Ai S. A novel photoelectrochemical sensor based on PPIX-functionalized WO₃-rGO nanohybrid-decorated ITO electrode for detecting cysteine. *Biosensors and Bioelectronics*. 2013; 44:48–51. doi: [10.1016/j.bios.2013.01.014](https://doi.org/10.1016/j.bios.2013.01.014) PMID: [23391706](https://pubmed.ncbi.nlm.nih.gov/23391706/)
37. Rajagopalan B, Chung JS. Reduced chemically modified graphene oxide for supercapacitor electrode. *Nanoscale research letters*. 2014; 9(1):1–10.
38. Ye H, Park HS, Bard AJ. Screening of electrocatalysts for photoelectrochemical water oxidation on W-doped BiVO₄ photocatalysts by scanning electrochemical microscopy. *The Journal of Physical Chemistry C*. 2011; 115(25):12464–70.
39. Han L, Guo S, Xu M, Dong S. Photoelectrochemical batteries for efficient energy recovery. *Chem Commun*. 2014; 50(87):13331–3.
40. Yu H, Wang J, Zhang S, Li X, Zhao H. Layered Fe (III) doped TiO₂ thin-film electrodes for the photoelectrocatalytic oxidation of glucose and potassium hydrogen phthalate. *Chinese Science Bulletin*. 2011; 56(23):2475–80.
41. Xie R, Su J, Li M, Guo L. Structural and photoelectrochemical properties of Cu-doped CdS thin films prepared by ultrasonic spray pyrolysis. *International Journal of Photoenergy*. 2013;2013.
42. Ikeda S, Nakamura T, Lee SM, Yagi T, Harada T, Minegishi T, et al. Photoreduction of water by using modified CuInS₂ electrodes. *ChemSusChem*. 2011; 4(2):262–8. doi: [10.1002/cssc.201000169](https://doi.org/10.1002/cssc.201000169) PMID: [21328555](https://pubmed.ncbi.nlm.nih.gov/21328555/)
43. Zang Y, Lei J, Hao Q, Ju H. "Signal-On" Photoelectrochemical Sensing Strategy Based on Target-Dependent Aptamer Conformational Conversion for Selective Detection of Lead (II) Ion. *ACS applied materials & interfaces*. 2014; 6(18):15991–7.
44. Bonaccorso F, Sun Z, Hasan T, Ferrari A. Graphene photonics and optoelectronics. *Nature photonics*. 2010; 4(9):611–22.
45. Cao A, Liu Z, Chu S, Wu M, Ye Z, Cai Z, et al. A Facile One-step Method to Produce Graphene–CdS Quantum Dot Nanocomposites as Promising Optoelectronic Materials. *Advanced materials*. 2010; 22(1):103–6. doi: [10.1002/adma.200901920](https://doi.org/10.1002/adma.200901920) PMID: [20217706](https://pubmed.ncbi.nlm.nih.gov/20217706/)
46. Yan J, Wang K, Liu Q, Qian J, Dong X, Liu W, et al. One-pot synthesis of Cd_xZn_{1-x}S-reduced graphene oxide nanocomposites with improved photoelectrochemical performance for selective determination of Cu²⁺. *RSC Advances*. 2013; 3(34):14451–7.
47. Pawar RC, Lee CS. Sensitization of CdS nanoparticles onto reduced graphene oxide (RGO) fabricated by chemical bath deposition method for effective removal of Cr (VI). *Materials Chemistry and Physics*. 2013; 141(2):686–93.
48. Neogi A, Karna S, Shah R, Phillipose U, Perez J, Shimada R, et al. Surface plasmon enhancement of broadband photoluminescence emission from graphene oxide. *Nanoscale*. 2014; 6(19):11310–5. doi: [10.1039/c4nr03055a](https://doi.org/10.1039/c4nr03055a) PMID: [25139261](https://pubmed.ncbi.nlm.nih.gov/25139261/)
49. Wang GL, Xu JJ, Chen HY. Selective detection of trace amount of Cu²⁺ using semiconductor nanoparticles in photoelectrochemical analysis. *Nanoscale*. 2010; 2(7):1112–4. doi: [10.1039/c0nr00084a](https://doi.org/10.1039/c0nr00084a) PMID: [20648335](https://pubmed.ncbi.nlm.nih.gov/20648335/)
50. Chen Y, Rosenzweig Z. Luminescent CdS quantum dots as selective ion probes. *Analytical Chemistry*. 2002; 74(19):5132–8. PMID: [12380840](https://pubmed.ncbi.nlm.nih.gov/12380840/)
51. Wang P, Ma X, Su M, Hao Q, Lei J, Ju H. Cathode photoelectrochemical sensing of copper (II) based on analyte-induced formation of exciton trapping. *Chem Commun*. 2012; 48(82):10216–8.
52. Isarov AV, Chrysochoos J. Optical and photochemical properties of nonstoichiometric cadmium sulfide nanoparticles: surface modification with copper (II) ions. *Langmuir*. 1997; 13(12):3142–9.
53. Wang J, Jiang X. Anodic near-infrared electrochemiluminescence from CdTe/CdS core small/shell thick quantum dots and their sensing ability of Cu²⁺. *Sensors and Actuators B: Chemical*. 2015; 207:552–5.
54. Konishi K, Hiratani T. Turn-On and Selective Luminescence Sensing of Copper Ions by a Water-Soluble Cd₁₀S₁₆ Molecular Cluster. *Angewandte Chemie International Edition*. 2006; 45(31):5191–4.
55. Yang P, Zhao Y, Lu Y, Xu QZ, Xu XW, Dong L, et al. Phenol formaldehyde resin nanoparticles loaded with CdTe quantum dots: a fluorescence resonance energy transfer probe for optical visual detection of copper (II) ions. *ACS nano*. 2011; 5(3):2147–54. doi: [10.1021/nn103352b](https://doi.org/10.1021/nn103352b) PMID: [21344860](https://pubmed.ncbi.nlm.nih.gov/21344860/)

56. Yantasee W, Lin Y, Fryxell GE, Busche BJ. Simultaneous detection of cadmium, copper, and lead using a carbon paste electrode modified with carbamoylphosphonic acid self-assembled monolayer on mesoporous silica (SAMMS). *Analytica Chimica Acta*. 2004; 502(2):207–12.
57. Soleimani M, Afshar MG. Potentiometric Sensor for Trace Level Analysis of Copper Based on Carbon Paste Electrode Modified With Multi-walled Carbon Nanotubes. *Int J Electrochem Sci*. 2013; 8:8719–29.
58. Kudr J, Nguyen HV, Gumulec J, Nejd L, Blazkova I, Ruttkay-Nedecky B, et al. Simultaneous Automatic Electrochemical Detection of Zinc, Cadmium, Copper and Lead Ions in Environmental Samples Using a Thin-Film Mercury Electrode and an Artificial Neural Network. *Sensors*. 2014; 15(1):592–610. doi: [10.3390/s150100592](https://doi.org/10.3390/s150100592) PMID: [25558996](https://pubmed.ncbi.nlm.nih.gov/25558996/)